13th World Conference on Earthquake Engineering
Vancouver, B.C., Canada
August 1-6, 2004
Paper No. 23

ESTIMATION OF INCIDENT SEISMIC WAVE BASED ON EFFECTIVE STRESS ANALYSIS

Hisakazu SAKAI[1], Sumio SAWADA[2]

SUMMARY

We propose a methodology to retrieve the up-going (incident) component of ground motion from borehole records by applying a backward calculation based on an effective stress analysis. Most of the available techniques to date are based on an equivalent linear analysis that is not accurate in cases of strong non-linearity. Numerical examples are conducted to examine the accuracy of the identified incident wave in cases of liquefaction. It is concluded from the results as follows: 1) The incident wave, as well as the stress-strain hysteresis and effective stress path of a liquefied layer, is retrieved from the noiseless record with high accuracy. 2) In case the observed record is not given at the sufficient depth, the accuracy of identified incident wave will decrease. 3) The proposed methodology can be applied to the records with white noise.

INTRODUCTION

The estimation of an incident wave is necessary for earthquake response analyses of a soil-structure system to study the damaged process of structures. The up-going (incident) component of ground motion needs to be retrieved from actual earthquake records for the purpose. Most of the available techniques to date are based on an equivalent linear analysis like the computer program "SHAKE" [1] that is not accurate in cases of strong non-linearity. Sugito et al. [2] and Yoshida et al. [3,4] modified the "SHAKE" code for applying to a large strain level. However, these methods still compute the ground non-linearity using the equivalent linear approximation. On the other hand, several identification methodologies were proposed for estimation of the incident wave in time domain considering the non-linearity of the soil. Toki et al. [5] and Sudo et al. [6] identify the input ground motions for linear systems of 3-story structures using the Kalman filter and the EK-WLI method, respectively. Maruyama and Hoshiya [7] proposed a formulation to identify a non-linear single degree of freedom system, whereas the identification was performed only for a linear system. We have proposed a backward calculation method that retrieves the incident wave from an actual earthquake record according to the non-linear stress-strain relationship [8,9], and applied to a non-linear multi-degree of freedom system in order to confirm the utility of the method, whereas we cannot retrieve it from a record on ground surface due to the numerical instability [10]. These

[1] Researcher, Earthquake Disaster Mitigation Research Center, National Research Institute for Earth Science and Disaster Prevention, Kobe, Japan. Email:sakai@edm.bosai.go.jp
[2] Associate Professor, Disaster Prevention Research Institute, Kyoto University, Uji, Japan.

studies are based on the total stress analysis, therefore the calculated incident wave is not accurate at a site where liquefaction occurs. In this study, we apply the effective stress analysis for the method of backward calculation. Numerical examples are conducted to examine the accuracy of the retrieved incident wave.

METHODOLOGY

Equation of motion for backward calculation

The equation of motion of a multi-degree of freedom system considering excessive pore water pressure can be written as

$$\boldsymbol{M}\ddot{\boldsymbol{x}} + \boldsymbol{C}\dot{\boldsymbol{x}} + \boldsymbol{Fs}(\boldsymbol{x},\boldsymbol{u}) = -\boldsymbol{M}\boldsymbol{i}\ddot{z} \tag{1}$$

where $\boldsymbol{M}$ and $\boldsymbol{C}$ are the mass and the viscous damping matrices, $\boldsymbol{x}$ and $\boldsymbol{u}$ the nodal relative displacement and the excess pore water pressure vectors, respectively, $\boldsymbol{Fs}$ the non-linear restoring force vector which is a function of $\boldsymbol{x}$ and $\boldsymbol{u}$, $\boldsymbol{i}$ a vector whose all component are 1, and $\ddot{z}$ the incident seismic acceleration at the bedrock.

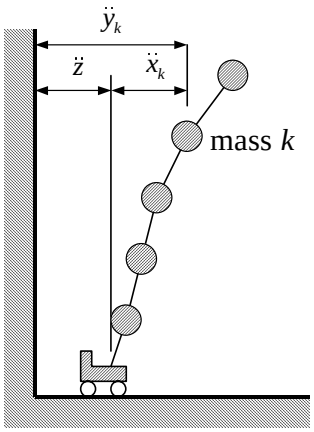

Figure 1. Relationships of the incident wave, relative acceleration and record wave at the observed point.

In a case that the absolute acceleration of mass k, $\ddot{y}_k$ is observed, it is related with $\ddot{z}$ and $\ddot{x}_k$ as follows:

$$\ddot{z} = \ddot{y}_k - \ddot{x}_k \tag{2}$$

where subscript k denotes the mass number.

The following equation is given by substituting Eq.(1) into Eq.(2):

$$\boldsymbol{M}\ddot{\boldsymbol{x}} + \boldsymbol{C}\dot{\boldsymbol{x}} + \boldsymbol{Fs}(\boldsymbol{x},\boldsymbol{u}) = -\boldsymbol{M}\boldsymbol{i}(\ddot{y}_k - \ddot{x}_k) \tag{3}$$

Moving the unknown parameters into the left side gives

$$\boldsymbol{M}'\ddot{\boldsymbol{x}} + \boldsymbol{C}\dot{\boldsymbol{x}} + \boldsymbol{Fs}(\boldsymbol{x},\boldsymbol{u}) = -\boldsymbol{M}\boldsymbol{i}\ddot{y}_k \tag{4}$$

$\boldsymbol{M}'$ is shown as follows:

$$M'_{ij} = M_{ij} - \sum_{l=1}^{N} M_{il}\delta_{jk} \tag{5}$$

where M'_{ij} and M_{ij} are ith-row and jth-colomn components of $\boldsymbol{M'}$ and $\boldsymbol{M}$, respectively, δ_{ij} Kronecker's delta, N the number of freedom.

Except the mass matrix of the left side and the input acceleration of the right side are different between Eqs.(1) and (4), these equations have the same terms. Therefore, we can calculate $\ddot{\boldsymbol{x}}$ and $\ddot{z}$ in Eq.(4) for all time steps using an ordinary time integration scheme.

Introduction of penalty function

It is known that the backward calculation method has an error with a rigid mode in the relative acceleration vector $\ddot{\boldsymbol{x}}$. In order to remove this error, we modify the acceleration as follows:

$$\ddot{\bar{\boldsymbol{x}}} = \ddot{\boldsymbol{x}} + \zeta \boldsymbol{i} \tag{6}$$

where $\ddot{\bar{\boldsymbol{x}}}$ denotes the final estimated acceleration vector at each time step and $\zeta \boldsymbol{i}$ a uniform acceleration vector error. ζ is obtained by applying the following objective function value minimum.

$$J = \sum_{i}^{N}\sum_{j}^{N} M_{ij}(\ddot{x}_i + \zeta - \ddot{\bar{x}}_i^{pre})^2 + \sum_{i}^{N}\sum_{j}^{N} M_{ij}\zeta^2 \tag{7}$$

where $\ddot{\bar{\boldsymbol{x}}}_i^{pre}$ denotes $\ddot{\bar{\boldsymbol{x}}}$ of ith-mass at the previous time step. In the objective function, we use the mass matrix as the weight for the relative accelerations.

NUMERICAL EXAMPLES

Constitutive model for effective stress analysis

We use the Shamoto's model involving the soil properties of liquefaction and cyclic mobility [11] for the effective stress model. The simulations are performed under undrained condition.

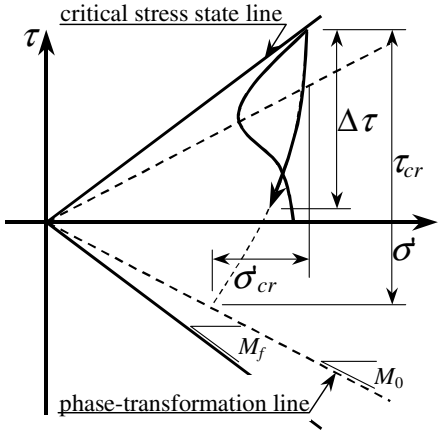

Figure 2. Effective stress process.

Stress-strain relationship

We use the Ramberg-Osgood model [12] for the stress-strain relationship combined with the Masing rule for defining the hysteresis loop. The incremental expression of the model is as follows;

$$d\gamma = \frac{d\tau}{G_0}\left(1+\alpha\beta\left|\Delta\tau / G'_0\right|^{\beta-1}\right), \tag{8}$$

where γ is the shear strain, τ the shear stress and $\Delta\tau$ the incremental shear stress from the unloading point shown in Figure 2. α and β are estimated by Eqs.(9) and (10) and G_0 is initial shear modulus calculated by Eq.(11). We give G_0 in case of skeleton curve and $2G_0$ in case of hysteresis curve as G'_0 of Eq.(8).

$$\alpha = \left(2/\gamma_{rf}\right)^{\beta-1} \tag{9}$$

$$\beta = \frac{2+\pi h_{\max}}{2-\pi h_{\max}} \tag{10}$$

$$G_0 = G_{0i}\left(\sigma'_m/\sigma'_{mi}\right)^m \tag{11}$$

$$\gamma_{rf} = \gamma_{rfi}\left(\sigma'_m/\sigma'_{mi}\right)^{m_r} \tag{12}$$

where σ'_m is the mean effective stress, σ'_{mi} the initial mean effective stress, γ_{rf} the reference shear strain under σ'_m condition. The subscripts i of G_0 and γ_{rf} denote these values under a mean effective stress of σ'_{mi}. h_{max} is the maximum damping factor. m and m_r are constant parameters that define the dependence of the initial shear modulus and the reference shear strain on the mean stress. We use 0.5 for the both referring the results of previous studies [13,14].

Excessive pore water pressure

We calculate the excessive pore water pressure u by the following three methods according to the phases in which the effective stress path is staying.

1) Before the stress path firstly reaches the phase-transformation line, u is defined as

$$\frac{u}{\sigma'_{mi}} = \frac{2}{\pi}\arcsin\left(R_n^{1/2\alpha_f}\right) \tag{13}$$

where α_f is a parameter controlling the increment of excessive pore water pressure, R_n represents the accumulative progress for an initial liquefaction. Shamoto et al. [11] estimate it as

$$R_n = \sum\left(\frac{1}{n_i} - \frac{1}{n_{i-1}}\right) \tag{14}$$

$$n_i = 2\left(\frac{\Delta\tau}{2\sigma'_{mi}C_1}\right)^{1/C} \tag{15}$$

$$C_1 = \left(1/20\right)^C R_{20} \tag{16}$$

where R_{20} is a shear stress ratio triggering an initial liquefaction at 20th cycle, n the number of loading cycles, C denotes an inclination angle between the cyclic shear stress ratio and the number of cycles triggering an initial liquefaction on log-log plane [15].

2) In the loading phases once after the stress path reaches the phase-transformation line, the increase of excessive pore water pressure Δu is obtained as

$$\Delta u = -\frac{1}{M_f}\frac{|\tau/\sigma'_m| - M_0}{M_f - M_0}|d\tau| \tag{17}$$

where M_f and M_0 are inclinations of the critical stress state line and the phase-transformation line, respectively. (See Figure 2)

3) In the unloading phases after the effective stress path crosses the phase-transformation line, Δu is calculated as

$$\frac{\Delta u}{\sigma'_{cr}} = f\left(\sum\frac{\Delta\tau_c}{\sigma'_m}\right)\frac{2}{\pi}\arcsin\left(R_{nc}{}^{1/2\alpha_f}\right) \tag{18}$$

$$R_{nc} = \left(\frac{\Delta\tau}{\tau_{cr}}\right)^3 \tag{19}$$

where σ'_{cr} and τ_{cr} are the increments of the mean effective stress and the shear stress from the unloading point to the aiming point on the opposite phase-transformation line as shown in Figure 2. In order to fit the excessive pore water pressure and shear strain more precisely, we make a slightly modification for the function f of Eq.(18) from the original Shamoto's model, that is

$$f(\xi) = \left(1 + \frac{2}{3+\xi^2}\right)^{-1}. \tag{20}$$

Numerical simulations of hollow cylindrical torsional shear tests

We carry out several cases of simulations of hollow cylindrical torsional shear tests [16] to examine the performance of the effective stress model, as shown in Table 1. The shear stress-strain relationships and the effective stress paths between the numerical simulations and laboratory tests are compared in Figure 3 and Figure 4, respectively. We determine the parameters of the model that fit the results of the laboratory tests as shown in Table 1 and Table 2. The initial shear modulus, G_{0i}, is calculated by the following equation [17].

$$G_{0i} = 900\frac{(2.17-e)}{1+e}(\sigma'_{mi})^{0.4} \quad (\mathrm{kgf/cm^2}) \tag{21}$$

where e denotes the void ratio.

Table 1. Analyzed cases and uncommon parameters, R_{20} and γ_{ri}.

Case	1	2	3
Dr(%)	60	70	79
R_{20}(%)	19.5	22.0	26.0
γ_{ri}	2.00×10^{-4}	2.19×10^{-4}	2.40×10^{-4}

Table 2. Common parameters of all cases.

C	α_f	h_{max}	M_0	M_f	e_{max}	e_{min}
-0.11	0.80	0.28	0.64	0.86	0.977	0.605

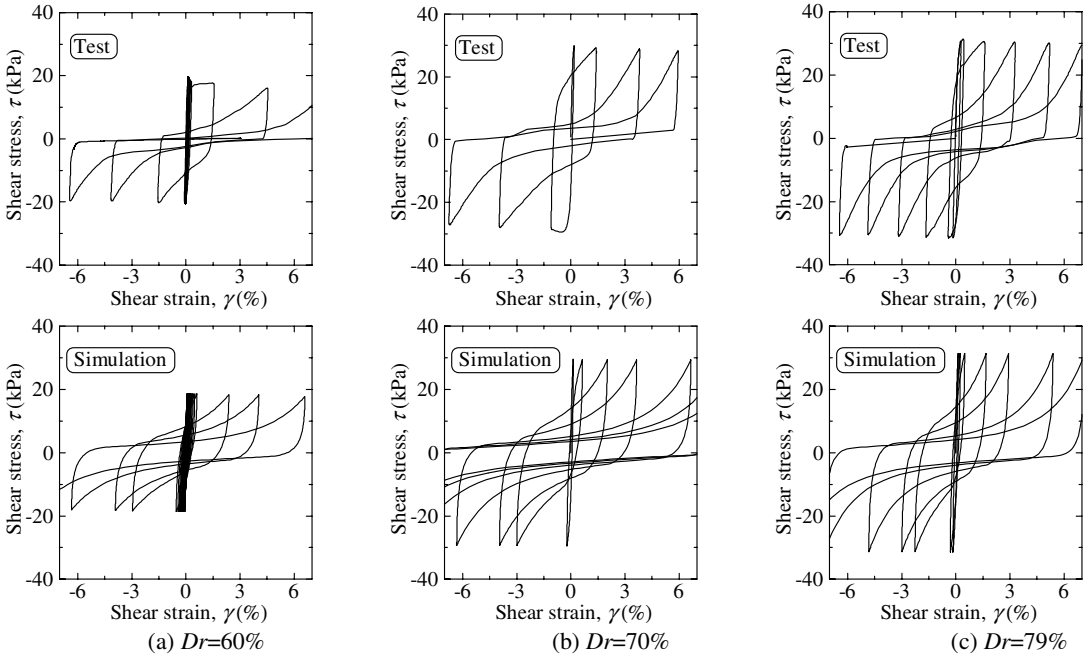

(a) Dr=60% (b) Dr=70% (c) Dr=79%

Figure 3. Comparison of the shear stress-strain relationships between the laboratory tests and the numerical simulations.

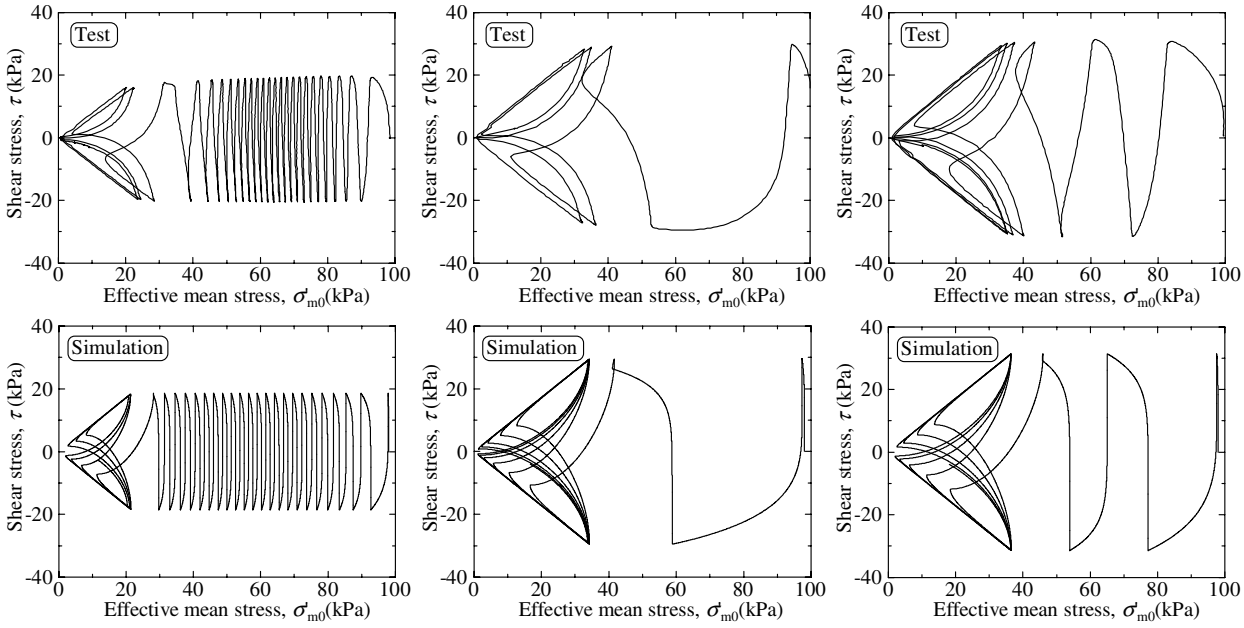

(a) Dr=60% (b) Dr=70% (c) Dr=79%

Figure 4. Comparison of the effective stress paths between the laboratory tests and the numerical.

Constitutive model for total stress analysis

Skeleton curve

Although Hardin-Drnevich model [18] and Ramberg-Osgood model [12] have been commonly used for the total stress models in the earthquake response analyses, these models are not able to represent the strain-dependency of shear modulus and damping factor accurately. Ishihara et al. [19], Kumasaki et al. [20], Nishimura and Murono [21] and Fukushima et al. [22] have recently proposed constitutive models for total-stress analysis based on the experimental results. The Fukushima's model is selected for the skeleton curve in this study, because it maintains a good agreement with the experimental results even in a large strain level by using a small number of parameters. The skeleton curve is shown as following equation;

$$\tau_i = \frac{G_{0i}\gamma_i}{1+\left|\gamma_i / \gamma_{rfi}\right|^{\delta_i}}, \tag{22}$$

where τ_i is the shear stress, G_{0i} the initial shear modulus, γ_i the shear strain, γ_{rfi} the reference strain whose subscripts i correspond to the component of ith-layer. δ_i is defined as

$$\delta_i = \delta_{Ai} \log_{10}(\gamma_i / \gamma_{rfi}) + \delta_{Bi}, \tag{23}$$

where δ_{Ai} and δ_{Bi} are the fitting parameters for the skeleton curve. In order to calculate the reference strain at a depth, the following equations are used considering the variation of stress-strain relations within a layer;

$$\gamma_{ri} = \tau_{ri} / G_{0i}, \tag{24}$$

$$\tau_{ri} = a_i + b_i \sigma_{mi}, \tag{25}$$

where τ_{ri} is the temporary strength parameter for calculating the reference strain, a_i and b_i are the strength and non-dimensional parameter, respectively, and σ_{mi} is the mean stress (K_0=0.5).

Hysteresis curve

We use the Ishihara's model [19] for defining the hysteresis curve. The model is based on the Masing rule with an imaginary shear modulus that varies for representing the damping factor obtained by the experiments. To reduce the large number of parameters the relationship between the damping factor and shear modulus is defined as

$$h_i = h_{\max i}(1 - G_i / G_{0i}) \tag{26}$$

where h_i is the damping factor and G_i the shear modulus calculated from the skeleton model described above.

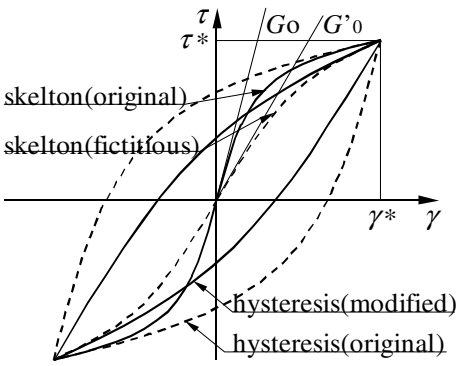

Figure 5. Modification of hysteresis curve.

Analyzed condition

Ground model

We retrieve the incident seismic waves from the absolute response accelerations at a certain depth in the ground that consists four layers including a liquefiable one as shown in Figure 6, where ρ is the mass density, V_{si} the initial shear velocity, D the depth from the surface (positive value). α_R and β_R are the Rayleigh damping constants related to mass and stiffness matrix, respectively. The ground model is divided into elements with 1m thickness, that is a 21 lumped masses system.

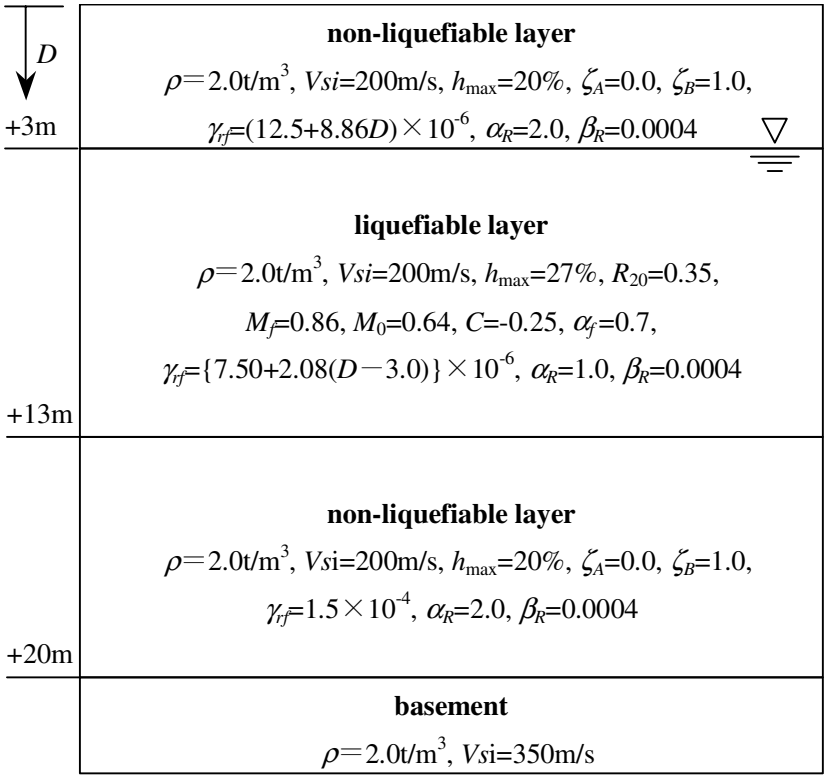

Figure 6. Analyzed ground model.

Incident seismic wave and absolute acceleration at basement level

In this study, we use the observed record at Port Island during 1995 Kobe earthquake [23] for the input motion. The forward calculation is performed to get the waveforms at G.L.-14m, -19m, -20m. Hereafter we call these waveforms as FCWs (FCW14, FCW19, FCW20). In the backward calculations, the former waveform is the target incident wave and the latter, FCWs, waveforms are assumed to be the observed records. They are shown in Figure 7 and Figure 8, respectively. We try to retrieve the incident wave from the FCWs assuming that all ground parameters in Figure 6 are known. The time interval is set to be 1/10,000 second for the forward and backward calculations.

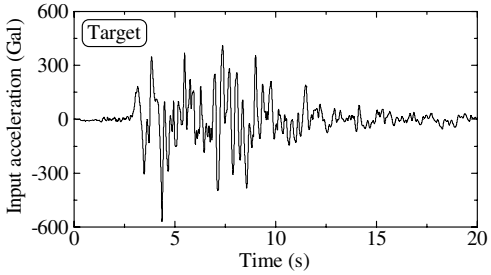

Figure 7. Test-incident waveform (Target).

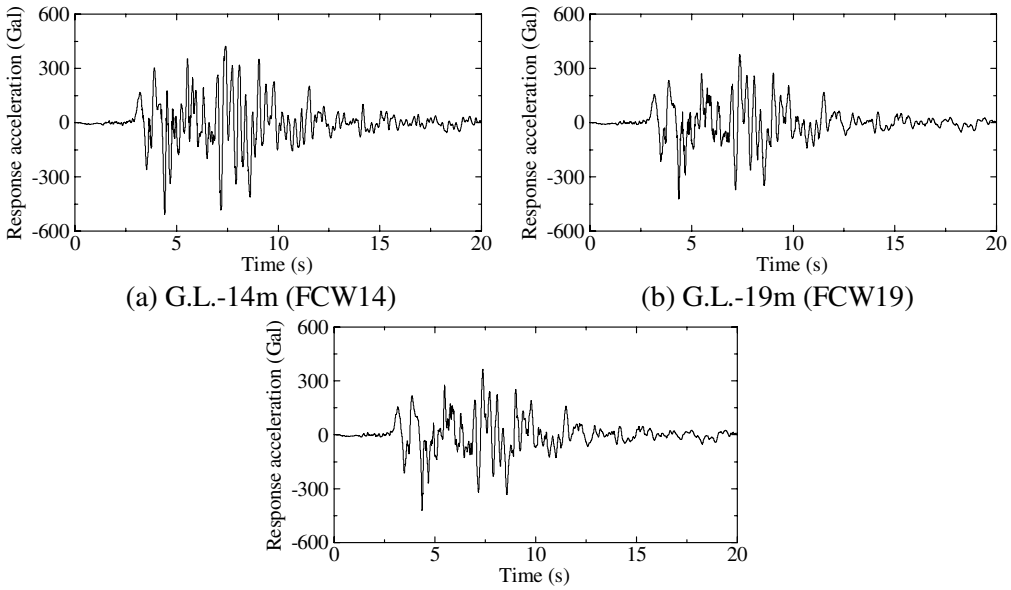

(a) G.L.-14m (FCW14)

(b) G.L.-19m (FCW19)

(c) G.L.-20m (FCW20)

Figure 8. Forward calculated waveforms (FCWs).

Accuracy of the retrieved incident wave

The retrieved incident wave from FCW20 is compared with the target waveform. In order to estimate the accuracy of the calculation, the following value is defined:

$$Er = \sum_{m=1}^{M} (\ddot{z}(m) - \ddot{\bar{z}}(m))^2 / \sum_{m=1}^{M} \ddot{z}^2(m) \tag{27}$$

where $\ddot{z}(m)$ and $\ddot{\bar{z}}(m)$ are the target and the retrieved incident accelerations at time m, respectively, and M the total number of time series.

The retrieved incident waveform is shown in Figure 9. The comparison of the stress-strain relationships and the effective stress paths between the forward and backward calculations in the element at the depth of 6.5m, which is in the liquefiable layer, are drawn in Figure 10 and Figure 11, respectively.

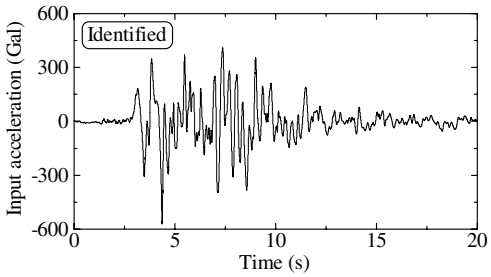

Figure 9. Incident waveform retrieved from FCW20.

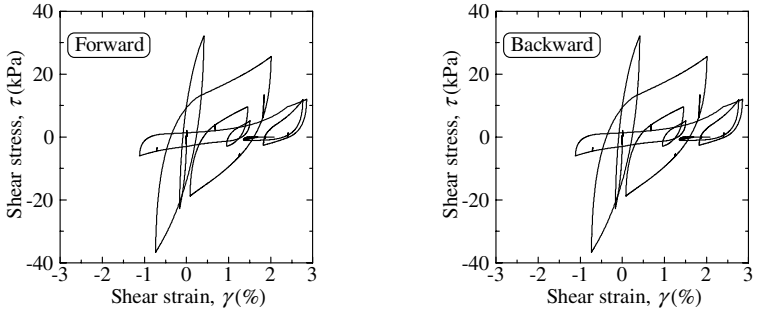

Figure 10. Stress-strain relationships at 6.5m depth.

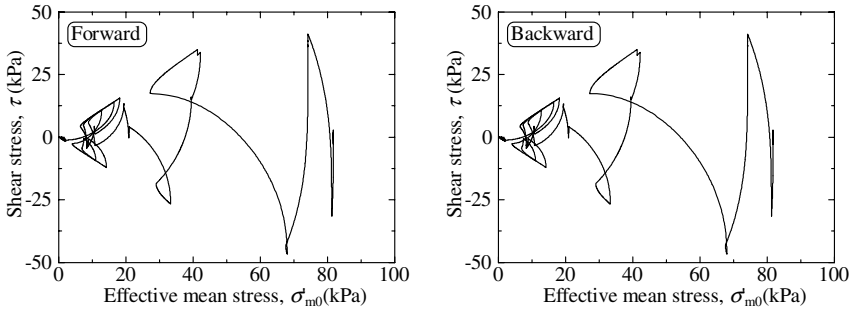

Figure 11. Effective stress paths relationships at 6.5 m depth.

We can observe that the retrieved waveform in Figure 9 agrees very well with the target one in Figure 7. The value of Eq.(27) is 1.3×10^{-5}. We can conclude from Figure 10 and Figure 11 that the stress-strain relationship and the effective stress path by the backward calculation are also simulated accurately even in the liquefied layer.

Effect of depth observed

We conduct numerical calculations to discuss the effect of the depth at which the seismic record observed. Figure 12 shows the retrieved incident waves from the FCW14 and FCW19.

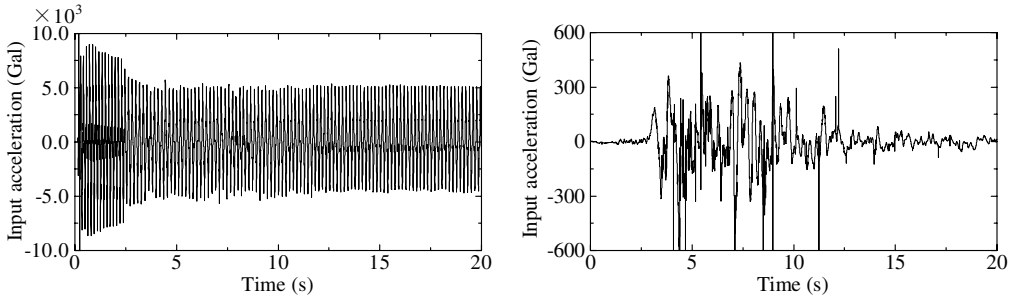

(a) G.L.-14m (FCW14) (b) G.L.-19m (FCW19)

Figure 12. Calculated incident waveforms.

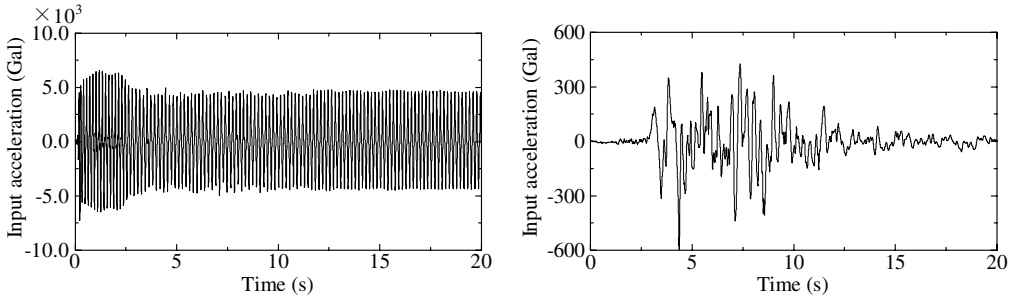

(a) G.L.-14m (FCW14) (b) G.L.-19m (FCW19)

Figure 13. Calculated incident waveforms through a low-pass-filter of 20Hz.

Figure 12 shows that the calculated incident wave from the FCW14 is not obtained properly. Note that the order of the retrieved incident wave is completely different from that of the target one. From FCW19 the incident waveform is successfully retrieved although it includes a high frequency noise. The error in high frequency range can be eliminated by a low-pass-filter of 20Hz as shown in Figure 13. However, we have the similar result from the record of G.L.-18m with Figure 13(a).

Robustness against noise

In order to investigate the robustness of the backward calculation against the observation noise, we try to retrieve the incident waves from FCW20 with white noises of 2%, 5% and 10% of the PGA. The square root of power ratios between noise and signal correspond to 1.8%, 4.7% and 10.3%, respectively. Figure 14 shows the waveforms of the FCW20 with noises.

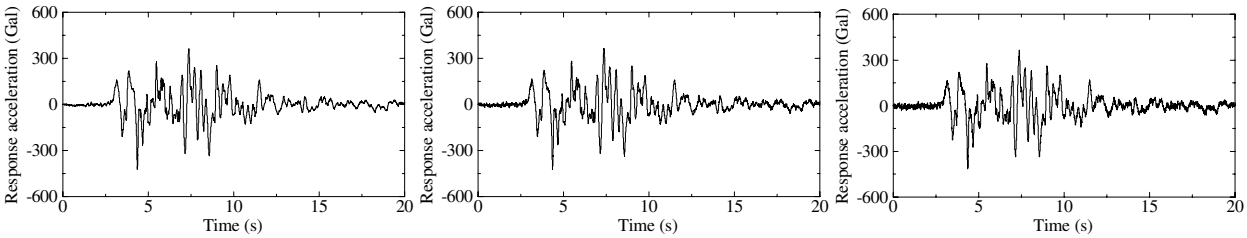

(a) 2% noise (b) 5% noise (c) 10% noise

Figure 14. Waveforms of FCW20 with noises.

Figure 15 and Table 3 show the retrieved incident waveforms and the error values *Er*, respectively. Figure 16 and Figure 17 show the stress-strain relationships and the effective stress path for 5% and 10% noises.

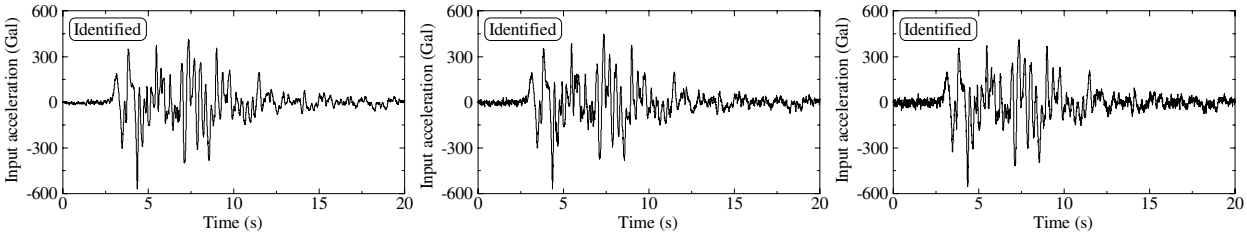

(a) 2% noise (b) 5% noise (c) 10% noise

Figure 15. Identified incident waveforms.

Table 3. Error estimation values.

noise	0%	2%	5%	10%
error function values : *Er*	1.3×10^{-5}	1.0×10^{-3}	2.4×10^{-2}	1.8×10^{-2}

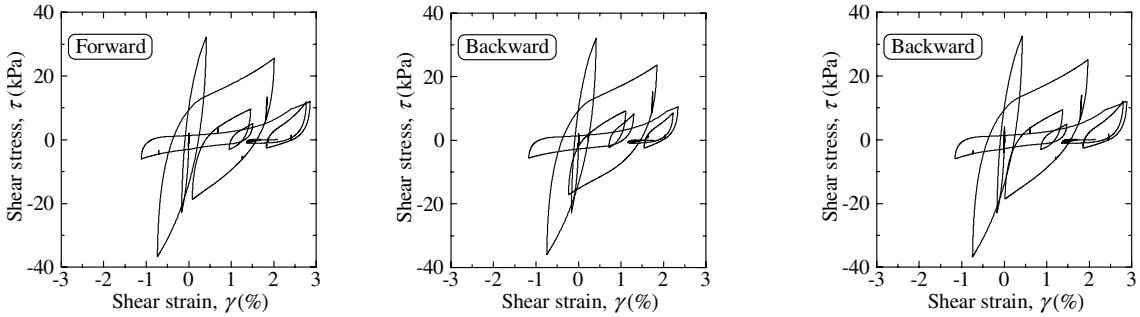

(a) Target (b) 5% noise (c) 10% noise

Figure 16. Shear stress-strain relationships.

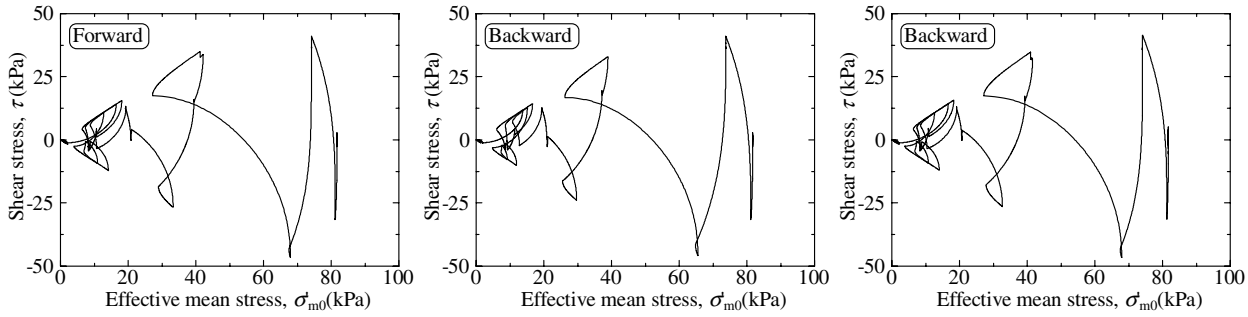

(a) Target (b) 5% noise (c) 10% noise

Figure 17. Effective stress paths.

In the case of 2% noise, the retrieved incident wave in Figure 15 agrees very well with the target one in Figure 7. It is also shown by *Er* in Table 3. In the cases of 5% and 10% noises, we can retrieve the

predominant part of the waveform of the incident waves with good accuracy, whereas the other parts include high frequency noise as shown in Figure 15(b) and (c).

The hystereses of the stress-strain relationships and effective stress are simulated precisely as shown in Figure 17. However, the mean effective stress decreases a little early and the shear strain from 1% to 3% is slightly different from the target in the case of 5% noise.

CONCLUSIONS

In this study, we introduce the effective stress analysis into the backward calculation method for identifying the incident seismic wave, and examine the accuracy and robustness of the method by performing numerical simulations using a ground model that includes a liquefiable layer. From these studies, we obtained the following results:

1) Numerical examples for retrieving the incident wave from the record at the base layer show that the calculated incident wave is a quit good agreement with the target as well as the stress-strain relationship and the effective stress path in the liquefied layer, under the condition that the ground parameters are known and the observed record do not contain any noise.

2) Numerical examples of the different recorded depths show that the accuracy of retrieved incident wave decrease as the observed depth becomes shallower. It means that the backward calculation method is useful for only retrieving the incident wave from the record observed in the base layer.

3) Numerical examples with the observation noises show that the retrieved incident waves maintain adequately precise whereas it includes a high frequency noise at the part in which the signal is small.

ACKNOWLEDGEMENTS

We are grateful to Y.Shamoto, N.Yoshida, M.Yoshizawa and H.Arai for giving useful advises and providing information about the effective stress analysis. We also extend out thanks to S.Kobayashi for providing the results of the hollow cylindrical torsional shear tests.

REFERENCES

1. P.B.Schnabel, J.Lysmer and H.B.Seed, "SHAKE - A computer program for earthquake response analysis of horizontally layered sites", *EERC Report*, vol.72, no.12, University of California, Berkley, 1972.
2. M.Sugito, Y.Goda and T.Masuda, "Frequency dependent equi-linearized technique for seismic response analysis of multi-layered ground" (in Japanese), *Journal of Geotechnical Engineering*, no.493, pp.49-58, 1994.
3. N.Yoshida and I.Suetomi, "DYNEQ: a computer program for dynamic analysis of level ground based on equivalent linear method" (in Japanese), *Reports of Engineering Research Institute, SatoKogyo Co., Ltd.* ,pp.61-70, 1996.
4. S.Nakamura and N.Yoshida, "Proposal of nonlinear earthquake response analysis in frequency domain considering apparent frequency dependency of soil property" (in Japanese), *Journal of Geotechnical Engineering*, no.722, pp.169-187, 2002.
5. K.Toki, T.Sato and J.Kiyono, "Identification of structural parameters and input ground motion from response time histories" (in Japanese), *Journal of structural mechanics and earthquake engineerin*g, no.410, pp.243-251, 1989.

6. A.Sudo, M.Hoshiya and I.Yanagawa, "Identification of an input and parameters of a MDOF system" (in Japanese), *Journal of Structural Engineering*, vol.41A, pp.709-716, 1995.
7. O.Maruyama and M.Hoshiya, "Identification of an input ground motion to a structure" (in Japanese), *Proceedings of the 19th JSCE Earthquake Engineering Symposium*, pp.145-148, 1987.
8. H.Sakai, S.Sawada and K.Toki, "A basic study to identify the incident wave on the base layer in time domain" (in Japanese), *Journal of structural mechanics and earthquake engineering*, no.577, pp.53-64, 1997.
9. H.Sakai, S.Sawada and K.Toki, "Identification of incident seismic wave in time domain considering non-linear behavior of soil", *Proceedings of Second International Conference on Earthquake Geotechnical Engineering*, vol.1, pp.193-198, 1999.
10. H.Sakai, S.Sawada and K.Toki, "A non-linear backward calculation to identify the incident wave at Port Island", (in Japanese), *Journal of structural mechanics and earthquake engineering*, no.612, pp.373-378, 1999.
11. Y.Shamoto, K.Tokimatsu and K.Ariizumi, "Applicability of a one-dimensional effective stress analysis to an existing soil deposit" (in Japanese), *Journal of Structural and Construction Engineering*, *AIJ*, no.433, pp.113-119, 1992.
12. P.C.Jennings, "Periodic response of a general yielding structure", *Journal of the Engineering Mechanics Division*, *ASCE*, vol.90, no.EM2, pp.131-163, 1964.
13. T.Kokusho, "Dynamic soil properties and nonlinear seismic response of ground" (in Japanese), *Journal of Geotechnical Engineering*, no.301, pp.176-306, 1982.
14. K.Sasaki and T.Iwasahi, "Dynamic soil properties -Dynamic soil properties for earthquake response analysis-" (in Japanese), *Tsuchi-to-Kiso*, *Japanese Geotechnical Society*, pp.85-91, 1985.
15. Y.Shamoto and K.Shimizu, "The applicability of a one-dimensional liquefaction analysis with cyclic mobility to loose and dense sand layer" (in Japanese), *Proceedings of 7th Japan Earthquake Engineering Symposium*, pp.685-690, 1986.
16. S.Kobayashi, "An study on dilatancy and volumetric change properties of sand during cyclic loading" (in Japanese), *Master thesis, Hokkaido University*, 2000.
17. T.Iwasaki and F.Tatsuoka, "Effects of grain size and grading on dynamic shear moduli of sands", *Soil and Foundations*, vol.17, no.3, pp.19-35, 1977.
18. B.O.Hardin and V.P.Drnevich, "Shear modulus and damping in soils, Measurement and parameter effects", *Journal of the soil mechanics and foundations division*, *ASCE*, vol.98, no.SM6, pp.603-624, 1972.
19. K.Ishihara, N.Yoshida and S.Tsujino, "Modeling of stress-strain relations of soils in cyclic loading", *Proceedings of 5th international conference on numerical methods in geomechanics*, pp.373-380, 1985.
20. I.Kumasaki, T.Sugiyama, M.Ueda, H. Hasegawa, "Hysteresis model considering strain dependency of momentary deformation modulus" (in Japanese), *Proceedings of annual conference of the JSCE*, vol.53(3A), pp.176-177, 1998.
21. A.Nishimura and Y.Murono, "Verification of stress-strain model for non-linear analysis of L2 earthquake motion" (in Japanese), *Proceedings of annual conference of the JSCE*, vol.54(1B), pp.226-227, 1999.
22. K.Fukushima, S.Goto, S.Okamoto and K.Sakashita, "Non-linear behaviors of sand at large levels of shear strain" (in Japanese), *Proceedings of annual conference of the JSCE*, vol.53(3A), pp.314-315, 1998.
23. Coastal Development Institute of Technology, "Handbook of countermeasures against liquefaction of landfill sites" (in Japanese), 1997.